Published by
NIGERIAN SOCIETY OF PHYSICAL SCIENCES
Available online @ https://journal.nsps.org.ng/index.php/jnsps

J. Nig. Soc. Phys. Sci. 8 (2026) 3355

Journal of the Nigerian Society of Physical Sciences

# Studies on the effects of kaolin filler concentrations on the thermal and mechanical performance of furan–lignin foam formulations

Alaba Joseph Adebayo*, Ilemobayo Ifedayo Oguntimehin

*Department of Chemical Sciences, Olusegun Agagu University of Science and Technology, P.M.B. 353, Okitipupa, Nigeria*

## Abstract

Plant-based furan–lignin foams (FLFs) offer several advantages over petroleum-based foams, including abundant and affordable feedstocks, fire resistance, thermal performance, environmental compatibility, and renewable origin. In this work, rigid plant-derived furan–lignin foams were synthesized by incorporating kaolin filler into the formulation. The effects of kaolin concentration (0, 0.5, 1.0, 1.5, 2.0, and 2.5 g, corresponding to foams KF1–KF6) on the thermal and mechanical properties of the foams were evaluated. Fourier transform infrared spectroscopy (FTIR), scanning electron microscopy (SEM), density measurement, compressive strength testing, thermogravimetric analysis (TGA), and derivative thermogravimetry (DTG) were used to characterize the kaolin-reinforced furan–lignin bio-based foams. The foams were high-density materials, and KF4, containing 1.5 g of kaolin, showed the best overall performance, with a density of 0.256 g/cm$^3$ and a compressive stress of 26.63 MPa. KF4 also exhibited promising thermal stability up to about 588.39 °C and a residue content of 19.48% at 863 °C. SEM analysis showed both open- and closed-cell morphologies, with cell sizes ranging from 40 to 250 $\mu$m. The results indicate that optimum kaolin loading can enhance the mechanical efficiency and thermal stability of rigid bio-based foams.

DOI: 10.46481/jnsps.2026.3355

*Keywords:* Kaolin, Furan–lignin foam, Bio-based foam, Thermal stability, Compressive strength

*Article History:*
Received: 11 March 2026
Received in revised form: 25 April 2026
Accepted for publication: 24 June 2026
Available online: 29 July 2026



Communicated by: E. A. Emile

## 1. Introduction

Polyurethane (PU) foams are widely used as sound and thermal insulation materials and as comfort-providing materials [1, 2]. The mechanical properties of these foams often require improvement because they do not always satisfy industrial requirements. Various fillers have been used for chemical or physical reinforcement. Fillers improve the rigidity, thermal and chemical resistance, compressive strength, and tensile strength of PU composites and, in many cases, lower production costs [3]. Fillers may be inorganic materials, such as natural minerals and glass beads, or organic materials, such as melamine and natural fibers. Inorganic materials are frequently used as fillers in polymer matrices, primarily to improve the mechanical strength, rigidity, and thermal resistance of composites [4]. Examples of such mineral fillers include silica, zeolite, diatomite, and clay minerals [4, 5].

Traditional PU foams are produced from isocyanates and polyols derived from petrochemical feedstocks, which creates several drawbacks. In addition to environmental and health concerns, synthetic polyols, isocyanates, additives, and fillers

*Corresponding author Tel. No.: +234-806-620-0476.
*Email address:* aj.adebayo@oaustech.edu.ng (Alaba Joseph Adebayo)

used in PU foam production can have further adverse effects. Petroleum-based chemicals are not sustainable, their costs are unstable, and workers in PU foam manufacturing facilities may experience health problems associated with the feedstocks and processing chemicals [6, 7]. Consequently, researchers and manufacturers are increasingly seeking bio-based and environmentally friendly alternatives to conventional polyols, isocyanates, fillers, and additives. Tighter regulations and increasing environmental awareness are driving this transition and highlighting the need for sustainable feedstocks for the development and reinforcement of rigid foams [6, 7].

The production and reinforcement of conventional and bio-based foams have been examined in several studies, including tannin/furanic foams without blowing agents and formaldehyde [8], jute-fiber-reinforced concrete [9], glass-fiber effects on kaolinite-based thermal insulators [10], natural-fiber-reinforced foamed concrete [11], bentonite-filled polyurethane composites [12], wood-fiber-reinforced composite foams [13], and lignin-reinforced tannin/furanic foams [14].

### *1.1. Current knowledge gaps*

Although interest in bio-based foams has increased, important gaps remain in understanding how inorganic fillers such as kaolin affect furan–lignin foams. In particular, limited empirical information is available on filler dispersion, matrix–filler interfacial interactions, and the influence of kaolin on foam formation, thermal behavior, mechanical performance, structural morphology, and optimum filler loading. Addressing these gaps is important for developing environmentally friendly, high-performance bio-based foams.

### *1.2. Novelty of the study*

Comparatively little attention has been devoted to the reinforcement of furan–lignin foams (FLFs), despite their growing relevance as sustainable polymeric materials. Recent studies have reported the production of rigid bio-based foams from furfuryl alcohol (FA) obtained from corncob residues and from lignin-based polyols synthesized from palm kernel shells [15, 16]. However, reinforced FLF systems remain largely unexplored. In particular, foam composites based on lignin-derived polyols from coconut shell and FA incorporating kaolin as an inorganic reinforcing filler have not been reported in the literature. To the best of the authors' knowledge, no documented study has addressed the reinforcement of furan–lignin foams using kaolin. This study therefore introduces a class of bio-based composite foams by integrating kaolin into the furan–lignin matrix and provides insight into filler dispersion, mechanical performance, thermal stability, morphological evolution, and morphology–property relationships in these sustainable materials.

### *1.3. Objective of the study*

This study systematically investigates the synthesis and effects of varying kaolin filler loadings on the mechanical performance and thermal stability of kaolin-reinforced furan–lignin bio-based foams. Emphasis is placed on understanding how filler incorporation influences the structure–property relationships governing foam behavior.

## 2. Materials and methods

The polyol used in the present study was obtained from liquefied lignin extracted from coconut shell, as described by Adebayo *et al.* [16]. The lignin-based polyol was liquefied in polyethylene glycol (PEG) 400 and had a hydroxyl number of 480 mg KOH/g and a liquefaction yield of 90.22%. The residue content of the polyol was estimated to be 2.39%. The quality of the obtained bio-polyol was suitable for rigid bio-based foam synthesis. The 40% glyoxal solution, FA, sulfuric acid, and diethyl ether used in this study were obtained from Sigma-Aldrich. The kaolin used as the filler was obtained from the open market. Distilled water and analytical-grade chemicals were used throughout the experiment.

### *2.1. Kaolin-reinforced furan–lignin foam formulations*

As shown in Table 1, the polyol, FA, glyoxal, kaolin powder, distilled water, and diethyl ether were prepared. After thorough agitation of the mixture in a glass beaker with a mechanical stirrer, about 20 g of 30% sulfuric acid was added. The mixture was stirred again for about 30 s, and the gelling polymer content was quickly transferred into the foaming box. The formulation product was poured into an open-top metal box cavity to blow, cream, and harden. For the best foaming performance, a metal box was selected because of its rapid and uniform heat dissemination. The metal box was prepared using a modified technique [15–17] and measured $10 \times 10 \times 2.5$ cm$^3$. Mature foams were removed from the box and kept at room temperature (25 °C) for three days before characterization. The suggested reaction mechanism is shown in Figure 1, and the produced foams are shown in Figure 2.

### *2.2. Determination of foam density*

Using DIN EN 323 (1993), the weights, lengths, widths, and thicknesses of the foams were measured in triplicate, and foam densities were calculated using Eq. (1):

$$\rho = \frac{z}{lbt}, \tag{1}$$

where $\rho$ is density, $z$ is the foam weight, and $l$, $b$, and $t$ are the length, breadth, and thickness of the reinforced foam, respectively.

### *2.3. Compressive strengths of the kaolin-reinforced furan–lignin foams*

The produced kaolin-reinforced furan–lignin foams were subjected to stress–strain tests using an Instron universal testing instrument (model 3369) in accordance with ASTM D 1621-04, a plane-wise compression test for foam materials. Under ambient conditions, the direction of loading was parallel to the direction of foam rise, consistent with commonly used test standards in the literature [18–20]. A computer attached to the testing instrument recorded the force and cross-head deformation in accordance with the standard guidelines. The width, length, and

Table 1: Formulations of kaolin-reinforced furan–lignin foams.

| Foam ID | Furfuryl alcohol (g) | Lignin-based polyol (g) | Water (g) | Glyoxal (g) | Diethyl ether (g) | Kaolin (g) | Sulfuric acid catalyst (g) |
|---|---|---|---|---|---|---|---|
| KF1 | 30 | 5 | 5 | 10 | 15 | 0 | 20 |
| KF2 | 30 | 5 | 5 | 10 | 15 | 0.5 | 20 |
| KF3 | 30 | 5 | 5 | 10 | 15 | 1.0 | 20 |
| KF4 | 30 | 5 | 5 | 10 | 15 | 1.5 | 20 |
| KF5 | 30 | 5 | 5 | 10 | 15 | 2.0 | 20 |
| KF6 | 30 | 5 | 5 | 10 | 15 | 2.5 | 20 |

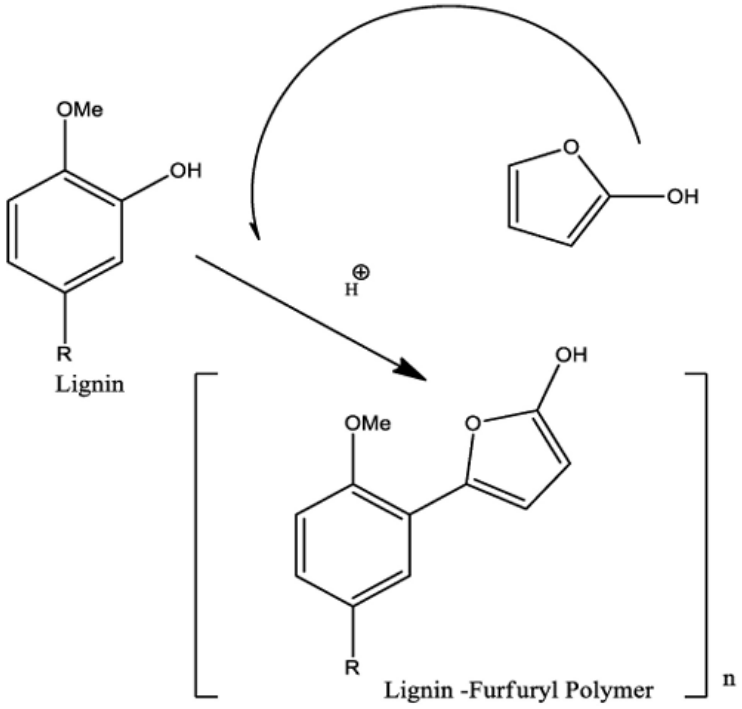


Figure 1: Suggested reaction mechanism for furfuryl alcohol and the phenolic component of lignin under acidic conditions [15].

Table 2: Densities and compressive stresses of kaolin-reinforced furan–lignin foams.

| Foam ID | Density (g/cm$^3$) | Compressive stress (MPa) |
|---|---|---|
| KF1 | 0.254 ± 0.013 | 0.84 ± 0.04 |
| KF2 | 0.241 ± 0.012 | 3.07 ± 0.15 |
| KF3 | 0.222 ± 0.011 | 18.63 ± 0.93 |
| KF4 | 0.256 ± 0.013 | 26.63 ± 1.33 |
| KF5 | 0.254 ± 0.0098 | 1.32 ± 0.07 |
| KF6 | 0.254 ± 0.011 | 5.29 ± 0.27 |

Values are means of triplicate measurements ± standard deviation.

thickness of the foam specimens were $10 \times 10 \times 2.5$ cm, and the crosshead speed was 2.0 mm/min. The foam was compressed to 10% of its initial thickness by applying a force of 10 kN [17]. Three readings were obtained for each specimen to determine the average compressive stress.

### 2.4. FTIR characterization of the functional groups

The developed kaolin-reinforced furan–lignin bio-based foams were characterized by FTIR. Foam samples were mixed with KBr and ground into a homogeneous powder in an agate mortar to prepare pellets. Spectra between 4000 and 500 cm$^{-1}$ were recorded using a PerkinElmer 3000 MX spectrometer. Each spectrum was collected at a resolution of 4 cm$^{-1}$. The infrared spectra were analyzed using Win-IR Pro Version 3.0, with a peak sensitivity of 2 cm$^{-1}$.

### 2.5. Morphology of the kaolin-reinforced furan–lignin foams

Scanning electron microscopy was used to investigate cell images and the microstructure of the furan–lignin foams reinforced with kaolin. A JEOL JSM 7600F scanning electron microscope with energy-dispersive X-ray spectroscopy (SEM–EDX) and an acceleration voltage of 10 kV was used. Cell-size distribution was quantified using ImageJ software. The embedded scale bars in the SEM images were calibrated, the images were converted to binary format, and particle analysis was performed. Equivalent cell diameters were determined from a minimum of 100 cells for each sample and analyzed statistically.

### 2.6. Thermogravimetric analysis

The thermal resistance of the furan–lignin foams reinforced with kaolin was evaluated using thermogravimetric analysis

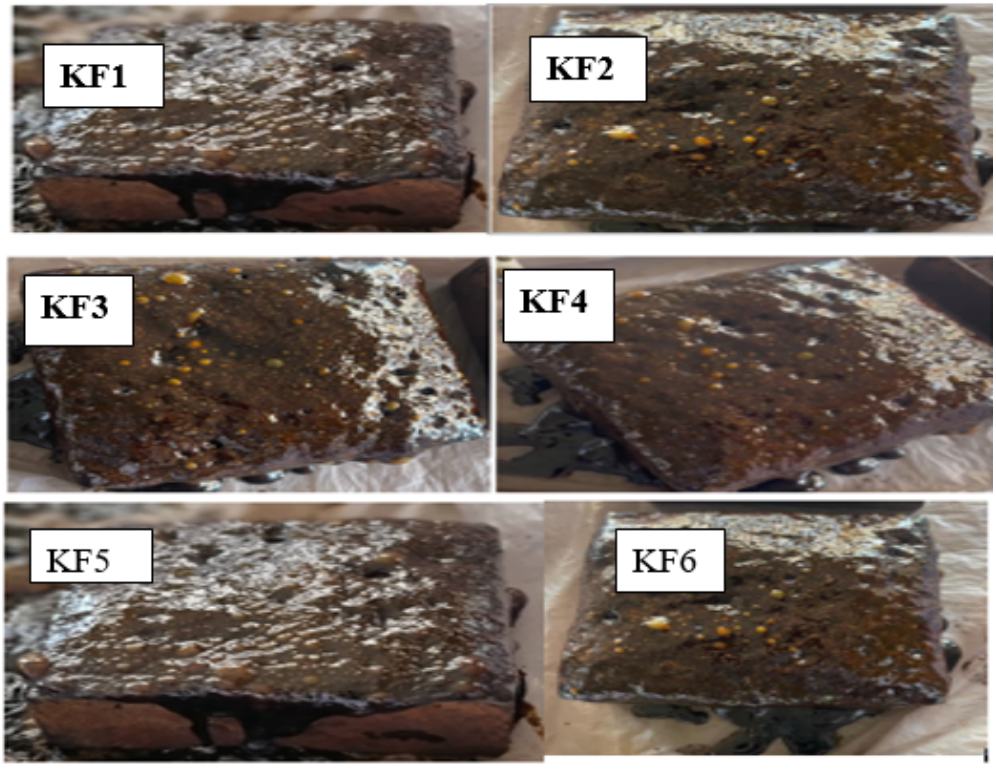


Figure 2: Images of the produced kaolin-reinforced furan–lignin foams.

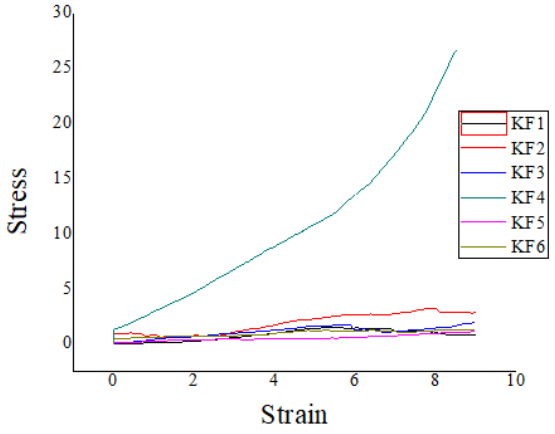


Figure 3: Behavior of kaolin-reinforced furan–lignin foams under compression.

Table 3: Relationship between the present thermal and mechanical properties and previous studies.

| Foam material | Compressive strength (MPa) | Density (g/cm$^3$) | $T_{max\,1}$ (°C) | $T_{max\,2}$ (°C) | $T_{max\,3}$ (°C) | Residue (%) |
|---|---|---|---|---|---|---|
| Tannin-based foams | 0.05–0.4 [28]; 0.00–0.170 [14] | 0.046–0.212 [14] | 72.1–84.9 [33] | 250.5–258.5 [33] | 315.3–326.7 [33] | 37.1–41.5 at 750 °C [33] |
| Lignin-based foams | 15.28–19.21 [15]; 14.00–18.86 [16] | 0.23–0.82 [15]; 0.2–0.9 [16] | 123.64–169.28 [15]; 123.64–158.30 [16] | 351.51–460.42 [15]; 346.42–450.69 [16] | 457.44–553.40 [15]; 443.58–586.09 [16] | 3.73–23.46 at 800 °C [15, 16] |
| Polyurethane foams | 0.14–9.08 [1]; 0.22–0.49 [3] | 0.029–0.038 [3] | 215–316 [3] | 314–340 [3] | 560–620 [3] | 0–20 at 1000 °C [3] |
| Current study | 0.84–26.63 | 0.22–0.26 | 251.88–448.50 | 289.54–501 | 371.22–588.39 | 19.14–23.85 at 863 °C |

(TGA) and derivative thermogravimetry (DTG). Before TGA testing, all foams were dried in an oven at 125 °C for 105 min to determine the true weight of each sample used for thermal-stability assessment. The foam samples were pulverized into

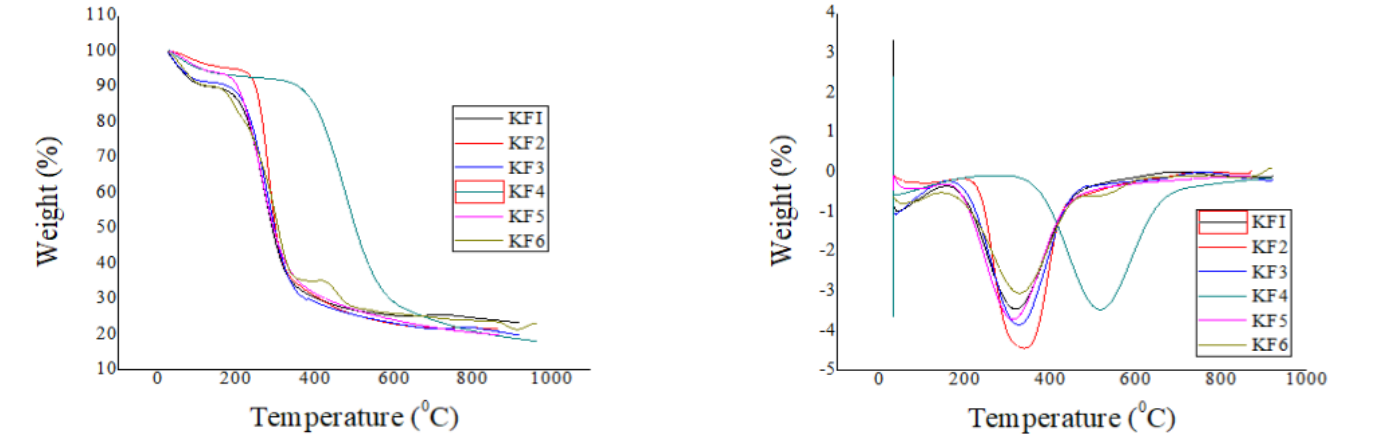


(a) TGA curves.

(b) DTG curves.

Figure 4: TGA and DTG curves of the produced kaolin-reinforced furan–lignin bio-based foams.

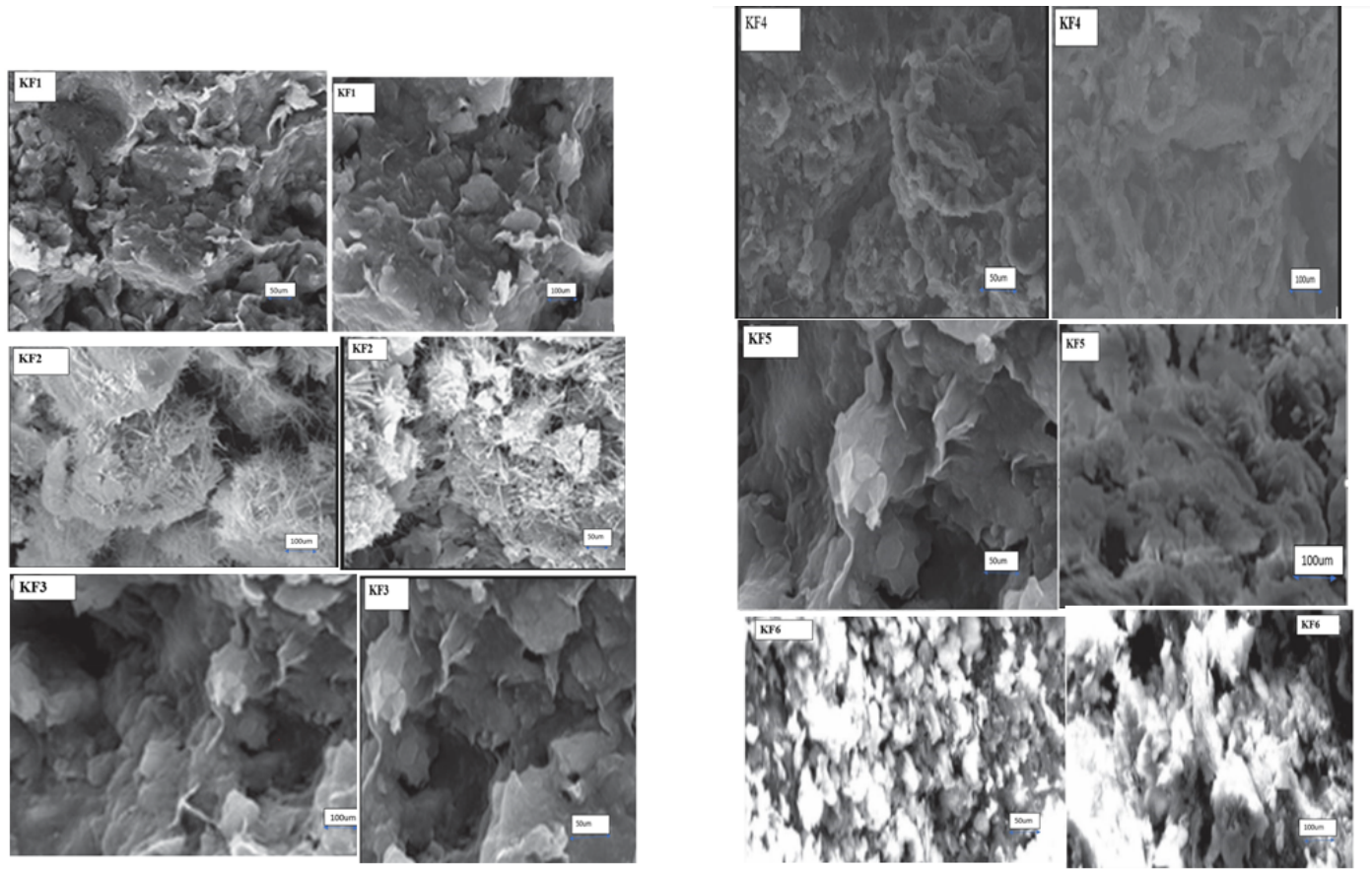


(a) SEM panels for KF1–KF6.

(b) Additional SEM panels for KF1–KF6.

Figure 5: SEM morphology of the produced kaolin-reinforced furan–lignin bio-based foams KF1–KF6.

fine powder and analyzed with a PerkinElmer TGA 4000 thermogravimetric analyzer. In each run, a 5 mg sample was heated at 10 °C/min from 25 to 900 °C under a constant nitrogen flow of 20 mL/min.

## 3. Results and discussion

### *3.1. Physical characteristics of the kaolin-reinforced furan–lignin foams*

Figure 1 illustrates the suggested reaction mechanism for the developed kaolin-reinforced furan–lignin foams, and Figure

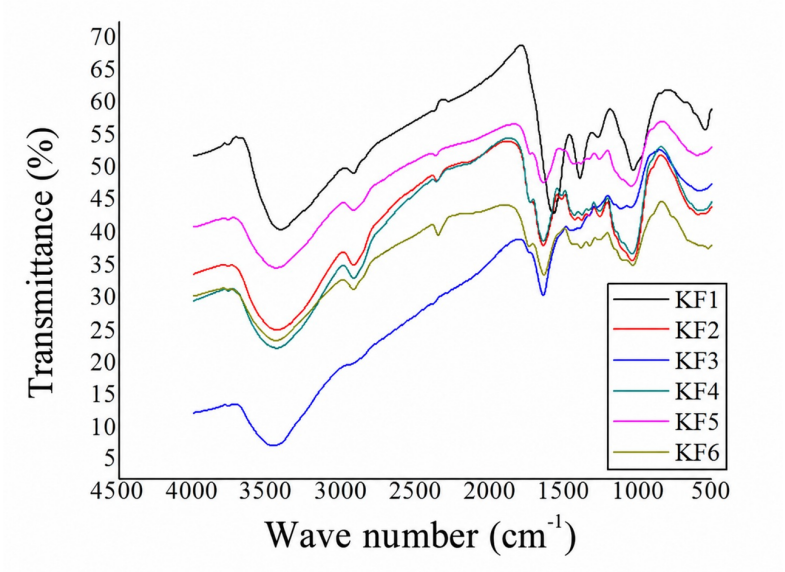


Figure 6: FTIR spectra of the produced kaolin-reinforced furan–lignin foams.

Table 4: TGA characteristics of furan–lignin foams reinforced with kaolin.

| Sample | $T_{max\,1}$ (°C) | $T_{max\,2}$ (°C) | $T_{max\,3}$ (°C) | Residue at 863 °C (%) |
|---|---|---|---|---|
| KF1 | 251.88 | 289.54 | 404.65 | 23.85 |
| KF2 | 275.88 | 297.40 | 409.26 | 21.48 |
| KF3 | 258.10 | 295.19 | 371.22 | 20.69 |
| KF4 | 448.50 | 501.00 | 588.39 | 19.48 |
| KF5 | 251.88 | 292.38 | 425.12 | 19.74 |
| KF6 | 258.10 | 304.28 | 465.90 | 23.39 |

2 shows the resulting foams. The compositions and variations in kaolin used as reinforcement in the foam formulations are presented in Table 1. The visual characteristics of the resulting foams appeared to be unaffected by changes in the amount of kaolin added during foam formation. Each foam's length and breadth were measured, and the volume was determined by multiplying the three dimensions. The densities of the resulting foams fell within a narrow range of 0.222–0.256 g/cm$^3$. The foams were generally high-density foams, with KF4 exhibiting the highest density (0.256 g/cm$^3$). The KF4 formulation contained 1.5 g of kaolin. As shown in Table 2, the foam densities were marginally lower at very high kaolin concentrations.

Kaolin is used as a filler in plastic materials because it can improve thermal stability, increase impact strength, enhance protection against chemical action and degradation, and assist in regulating flow properties. The density of PU foams has also been reported to improve when kaolin and dolomite are added to the formulations [21, 22]. However, no previous literature report was found on the addition of kaolin to furan–lignin foams or on the resulting behavior of kaolin-reinforced furan–lignin foams. Previous studies reported densities of 0.23–0.90 g/cm$^3$ for lignin-based foams [15, 16], 0.046–0.212 g/cm$^3$ for tannin-based foams [14], and 0.029–0.038 g/cm$^3$ for PU foams [3] (Table 3). The density range obtained in the present study was lower than those previously reported for lignin-based rigid bio-based foams but higher than those reported for PU and tannin-based rigid foams. This variation may arise from differences in the feedstock materials used to produce lignin-based polyols, because lignin characteristics are linked to feedstock source [17]. Although the exact amount of kaolin that optimizes furan–lignin foam density has not been established in the literature, the highest density in this study was obtained when 1.5 g of kaolin was added to the formulation (KF4). Various factors influence foam density, including the viscosity of the reacting mixture, blowing-agent evaporation rate, mixing efficiency, curing kinetics, and filler-dispersion quality. A highly viscous reacting mixture can limit bubble growth and produce high-density foams. Well-dispersed filler can improve nucleation and reduce density, whereas agglomerated filler dispersion can produce less dense foams.

### 3.2. *Compressive strengths of the kaolin-reinforced furan–lignin foams*

The compressive properties of the furan–lignin foams reinforced with kaolin are shown in Figure 3 and Table 2. The compressive stress ranged from 0.84 to 26.63 MPa. At the maximum deformation point, the final foam thickness was reduced to 10% of its original thickness. Stress–strain compression can cause densification, cell-wall disintegration, and cell-wall bending in elastic foams [15, 23, 24]. The results indicate that KF4, containing 1.5 g of kaolin, withstood the highest compressive stress before cell collapse. In contrast, KF1, KF2, KF3, KF5, and KF6 did not appear to display the same elastic-foam behavior. KF2 withstood stress up to 3.07 MPa before collapse, whereas KF4 gave the best performance under stress.

The behavioral differences in the rigid foams appear to be caused by variations in the kaolin concentration in their formulations [22]. KF4 showed the highest resistance to stress, had the highest density (0.256 g/cm$^3$), and sustained up to 26.63 MPa of stress before collapse. Previously reported compres-

Table 5: Estimated relative activation energy of furan–lignin foams reinforced with kaolin.

| Sample | Kaolin loading (g) | Relative activation energy (kJ/mol) | Implication of kaolin loading |
|---|---|---|---|
| KF1 | 0 | 90–130 | No barrier; heat penetrates easily, and low activation energy results in rapid degradation. |
| KF2 | 0.5 | 110–150 | Partial barrier formation provides some stabilization and a moderate increase in activation energy. |
| KF3 | 1.0 | 100–140 | Partial barrier formation provides some stabilization and a moderate increase in activation energy. |
| KF4 | 1.5 | 180–250 | Critical loading at which kaolin forms a thermal barrier that delays bond cleavage, suppresses diffusion of volatile materials, and promotes stable char formation. |
| KF5 | 2.0 | 120–160 | Agglomeration reduces effectiveness and causes the activation energy to decrease. |
| KF6 | 2.5 | 140–190 | Agglomeration reduces effectiveness, although a slight recovery is observed due to increased inorganic residue contribution (Table 4). |

Table 6: Estimated cell-size ranges of furan–lignin foams reinforced with kaolin.

| Sample | Kaolin loading (g) | Cell-size range ($\mu$m) | Morphology |
|---|---|---|---|
| KF1 | 0 | 120–250 | Coarse and irregular cells |
| KF2 | 0.5 | 80–150 | Improved and fibrous cells |
| KF3 | 1.0 | 60–120 | Compact and uniform cells |
| KF4 | 1.5 | 40–90 | Highly uniform optimum cells |
| KF5 | 2.0 | 90–180 | Agglomerated and distorted cells |
| KF6 | 2.5 | 100–200 | Heterogeneous cells |

sive stresses are 0.14–9.08 MPa for PU foams [3], 0.00–0.170 MPa for tannin-based foams [14, 28], and 14.00–19.21 MPa for lignin-based foams [15, 16] (Table 3). These results show that kaolin can increase the compressive strength of furan–lignin foams up to an optimum loading of 1.5 g. Beyond this loading, agglomeration and structural heterogeneity likely cause a substantial decrease in mechanical performance. The observed behavior underscores the importance of balancing filler reinforcement and dispersion quality in determining foam integrity.

The findings in Figure 3 and Table 2 demonstrate a clear association between foam density and compressive strength [14, 15]. Previous research has shown that denser foams generally exhibit higher compressive strengths [14, 22, 25–27]. Consequently, KF4 may be suitable for applications requiring higher load-bearing or impact-energy absorption, such as packaging for heavy electronics, high-impact packaging components, or automotive bumper applications.

### *3.3. Thermal stability of the kaolin-reinforced furan–lignin foams*

The thermal stability of the resulting kaolin-reinforced furan–lignin bio-based foams was assessed. The TGA and DTG curves are shown in Figure 4, and the thermal parameters are summarized in Table 4. The thermal properties, degradation pattern, and char-forming tendency of the developed kaolin-reinforced furan–lignin polymer foams were evaluated using TGA and DTG. The TGA profiles revealed a multistage degradation pattern characteristic of furan–lignin polymers reinforced with inorganic fillers.

At the first degradation stage, $T_{\max 1}$ ranged from 251.88 to 448.50 °C. KF4 showed delayed decomposition up to about 448.50 °C. The addition of kaolin to polyurethane foam formulations has previously been reported to minimize volatilization [22]. Table 3 summarizes thermal behavior reported for several foam materials. First-stage decomposition temperatures have been reported as 72.1–84.9 °C for tannin-based foams [33], 123.64–169.28 °C for lignin-based foams [15, 16], and 215–316 °C for PU foams [3]. The present data in Table 4 show that furan–lignin foams reinforced with kaolin exhibited slower thermal degradation at the first degradation stage.

The second degradation stage ranged from 289.54 to 501 °C (Table 4). Reported second-stage degradation ranges are 250.5–258.5 °C for tannin-based foams [33], 346.42–460.42 °C for lignin-based foams [15, 16], and 314–340 °C for PU foams [3]. According to the TGA curves (Figure 4) and Table 4, KF2 exhibited the earliest and most pronounced weight loss, indicating reduced thermal resistance. The decomposition trends of KF1, KF3, KF5, and KF6 were similar, indicating high crosslink density. KF4 retained greater mass up to 501 °C and showed a notable delay in degradation. The delayed degradation of KF4 relative to the other KF foams, lignin-based foams, tannin-based foams, and PU foams indicates that appropriate kaolin incorporation improves thermal resistance. Above 400 °C, degradation of the kaolin-reinforced furan–lignin foams decreased considerably, possibly because of the formation of strong aromatic-ring networks, lignin-derived char, and kaolin-filler structures in the polymer matrix.

The third and final degradation stage ranged from 371.22 to 588.39 °C (Table 4). Previously reported third-stage ranges are

560–620 °C for PU foams [3], 315–326.7 °C for tannin-based foams [33], and 443.58–586.09 °C for lignin-based foams [15, 16]. KF4 again demonstrated notable performance by degrading gradually rather than abruptly. However, porous thermal-insulation polyurethane foam materials reported by Ref. [3] showed better thermal performance than KF4 in the present study (Table 3). All KF foams in the present study retained considerable residual char contents of 19.48–23.85% at 863.03 °C (Table 4). Lignin-based foam materials have been reported to exhibit similar residual char contents of 3.73–23.46% at 800 °C [15, 16], whereas tannin-based foams and PU foams have reported residues of 37.10–41.50% at 750 °C [33] and 0–20% at 1000 °C [3], respectively. These results demonstrate the robust char-forming characteristics of lignin-rich materials. The formation of shielding carbon–ceramic structures, the thermal stability of the kaolin mineral phase, and carbonization of the aromatic lignin backbone may all contribute to elevated char residue. Higher residual char yield indicates improved thermal stability, insulating efficacy, and flame resistance.

The DTG profiles provide further insight into maximum degradation temperatures and degradation rates. Most samples showed notable DTG peaks between 300 and 380 °C, corresponding to the greatest rate of polymer-matrix degradation. KF2 had the strongest negative peak in Figure 4, indicating rapid thermal decomposition. The degradation rates of KF1, KF3, KF5, and KF6 were moderate. KF4 exhibited a broader and more complete shift of the DTG peak toward higher temperature, in the range of 500–600 °C. This shift suggests increased activation energy, improved thermal stability, and stronger filler–matrix interaction. Kaolin particles can promote catalytic carbonization, hinder mass movement, and act as a barrier to heat transfer, thereby reducing polymer-chain mobility and slowing degradation reactions. Figure 4 therefore indicates that 1.5 g is the optimum kaolin loading, because kaolin reinforcement and compatibility with the furan–lignin matrix are improved without severe filler clustering.

### 3.4. Kinetic insight into thermal degradation using the Arrhenius framework

For TGA decomposition, the Arrhenius framework in Eq. (2) relates the frequency factor $A$ to structural independence and molecular flexibility in the kaolin-reinforced furan–lignin foams. The activation energy, $E_a$, relates to the energy required to break bonds such as C–O–C bonds and aromatic structures:

$$k = A \exp\left(-\frac{E_a}{RT}\right), \tag{2}$$

where $A$ is the frequency factor, $\exp(-E_a/RT)$ is the fraction of molecular attempts that succeed, and $k$ is the reaction-rate constant. In foam degradation, $k$ represents the speed of decomposition at a given temperature. A small value of $k$ indicates low degradation and high thermal stability, whereas a large value of $k$ indicates rapid degradation and low thermal stability. The heating rate is denoted by $\beta$, and the DTG peak temperature is denoted by $T_p$. The Kissinger form used for comparative interpretation is given in Eq. (3):

$$\ln\left(\frac{\beta}{T_p^2}\right) = \ln\left(\frac{AR}{E_a}\right) - \frac{E_a}{RT_p}. \tag{3}$$

The TGA profiles show that degradation occurred in three stages, with the main decomposition taking place in the 200–350 °C temperature range because of the cleavage of ether, furan, and lignin linkages. The addition of kaolin strongly modified the degradation kinetics, as shown by changes in degradation temperatures and lower rates of mass loss. KF4 showed the greatest thermal stability, suggesting increased activation energy (Table 5) as a result of stronger interfacial interactions and the development of an effective inorganic barrier. This barrier limits heat transfer and the diffusion of volatiles, thereby retarding thermal degradation. At higher concentrations, particle agglomeration reduces this effect and decreases thermal resistance. The rate constant for degradation increases exponentially as temperature increases. Samples containing kaolin at the optimum level (KF4) showed lower rate constants at the same temperatures, suggesting increased thermal resistance.

### 3.5. SEM morphology of the kaolin-reinforced furan–lignin foams

Figure 5 and Table 6 show the SEM morphology results for the six developed furan–lignin foams reinforced with kaolin. The foams displayed both open- and closed-cell characteristics. KF1, which contained no kaolin and had a cell-size range of 120–250 $\mu$m, showed thick closed cells with fused and collapsed cell walls. It had a small number of distinct pores and few interconnected pores within dense polymer-matrix regions. Gas encapsulation during foam formation and curing was evident from the appearance of separated closed cells with limited interlinking regions. A comparable range of 20–200 $\mu$m has been reported for furan–lignin foams [15, 16].

KF2, containing 0.5 g of kaolin and having a cell-size range of 80–150 $\mu$m, showed open-cell foam characteristics with a fractured and heavily fibrous internal structure. Several interconnected voids with ruptured cell openings were observed. The foam showed widespread cell-wall rupture, creating continuous pore channels typical of open-cell polymer foams. KF3, containing 1.0 g of kaolin and having a cell-size range of 60–120 $\mu$m, showed predominantly semi-open cells with a broad, irregular pore pattern, partial wall rupture, and a mixture of intact and connected cells. Limited cell-wall damage permitted pore communication. KF4, containing 1.5 g of kaolin and having a cell-size range of 40–90 $\mu$m, behaved as an open-cell rigid foam with a sponge-like morphology, thread-like cell walls, continuous porous interlinks, and strong interconnectivity, indicating substantial gas release during foaming.

KF5, containing 2.0 g of kaolin and having a cell-size range of 90–180 $\mu$m, was primarily a closed-cell rigid foam, with localized voids and numerous closed apertures embedded in compacted regions with reduced pore connectivity. The polymer walls enclosed most pores. KF6, containing 2.5 g of kaolin and having a cell-size range of 100–200 $\mu$m, showed an open-cell rigid foam structure with clustered regions, continuous

void connections, and a largely fragmented cellular architecture. The SEM results show that the transition between open and closed morphologies is influenced by kaolin concentration. SEM micrographs of KF4 showed that kaolin particles were more evenly dispersed within the furan–lignin matrix, with limited agglomeration and strong interfacial adhesion, as indicated by the absence of pronounced particle pull-out and the presence of a rough fracture surface. Conversely, higher filler loadings showed stronger agglomeration, with large cluster-like domains and poorer dispersion. This reduced the effective interfacial area and created sites for stress concentration. The transition from a uniformly distributed to an aggregated microstructure accounts for the decline in mechanical properties at higher kaolin loadings. These findings demonstrate that kaolin loading affects enclosed-gas release, cell-wall rupture, and bubble stabilization during foam development.

### *3.6. FTIR characterization of the produced kaolin-reinforced furan–lignin foams*

FTIR spectroscopy was used to identify bonds formed during foaming of the kaolin-reinforced furan–lignin foams. The structural composition of foams KF1–KF6 and the reactions that occurred in the foams are shown in Figure 6. The spectra showed broad peaks at 3100–3500 $cm^{-1}$, which are characteristic of O–H or Al–OH stretching vibrations [14, 25, 30]. The broader O–H stretching in KF1, KF5, and KF3 indicates the presence of hydroxyl groups in the foam materials, whereas KF2, KF4, and KF6 showed less pronounced transmittance separation. The 1600–1550 $cm^{-1}$ bands may be attributed to aromatic rings from the benzene units of lignin-containing polyol or from furan rings [25, 31, 32]. Al–OH stretching around 915 $cm^{-1}$ may be attributed to the kaolinite peak. The absorption peak for ether (C–O–C) bonds at about 1033 $cm^{-1}$ is associated with condensation reactions between lignin-based polyol and FA and possibly between glyoxal and FA or lignin. Ether bonds can also form between FA molecules or lignin molecules through self-condensation under acidic conditions.

## 4. Conclusion

This study successfully demonstrated the synthesis of furan–lignin-based bio-foams reinforced with kaolin filler. Systematic variation in filler concentration produced six foam formulations (KF1–KF6). The foaming process occurred through acid-based autocondensation and a self-blowing mechanism, which generated sufficient exothermic heat to drive expansion and network formation. The results demonstrate the importance of kaolin concentration in determining the physical, mechanical, and thermal properties of the resulting foams. A nonlinear structure–property relationship was observed, indicating an optimum filler loading rather than a simple linear dependence. KF4, containing 1.5 g of kaolin, showed the best overall performance, including enhanced compressive strength, improved density and structural strength, optimized cellular morphology, and substantially improved thermal stability. These improvements are attributed to favorable kaolin dispersion and interaction within the polymer matrix, which promoted efficient stress transfer, reinforced the cell walls, and enhanced thermal-barrier properties. Lower kaolin contents (KF1–KF3) did not provide sufficient reinforcement, whereas higher kaolin contents (KF5–KF6) likely led to particle clustering and structural heterogeneity, thereby reducing performance. Microstructural assessment showed that KF4 had a more homogeneous and refined cellular structure, directly contributing to its mechanical and thermal performance. This demonstrates the close relationship between cell morphology and functional properties in bio-based foams. Overall, the present work provides insight into the development and optimization of lignin-based composite foams and highlights the importance of filler loading in the design of high-performance sustainable polymeric materials.

## Data availability

The data will be provided on request.

## Declaration of competing interest

The authors declare no competing interests in the preparation and dissemination of this work.

## Funding

The authors received no specific funding for this work.

## Acknowledgment

The authors express their gratitude to the Department of Chemical Sciences, Olusegun Agagu University of Science and Technology (OAUSTECH), Okitipupa, Nigeria, for providing the facilities required to carry out this research work.

## References

[1] M. C. Iacob, D. Popescu, C. Stochioiu, F. Baciu & A. Hadar, "Compressive behavior of thermoplastic polyurethane with an active agent foaming for 3D-printed customized comfort insoles", Polymer Testing **137** (2024) 108517. https://doi.org/10.1016/j.polymertesting.2024.108517.

[2] F. Campana, G. Brufani, F. Mauriello, R. Luque & L. Vaccaro, "Green polyurethanes from bio-based building blocks: recent advances and applications", Green Synthesis and Catalysis **6** (2025) 217. https://doi.org/10.1016/j.gresc.2024.08.001.

[3] Z. Wang, C. Wang, Y. Gao, Z. Li, Y. Shang & H. Li, "Porous thermal insulation polyurethane foam materials", Polymers **15** (2023) 3818. https://doi.org/10.3390/polym15183818.

[4] K. A. Ter-Zakaryan, A. D. Zhukov, E. Y. Bobrova, I. V. Bessonov & E. A. Mednikova, "Foam polymers in multifunctional insulating coatings", Polymers **13** (2021) 3698. https://doi.org/10.3390/polym13213698.

[5] T. W. M. Salih & L. A. A. Jawad, "Evaluating the thermal insulation performance of composite panels made of natural luffa fibres and urea-formaldehyde resin for buildings in the hot arid region", Advances in Building Energy Research **16** (2022) 696. https://doi.org/10.1080/17512549.2022.2098534.

[6] M. H. Tran & E. Y. Lee, "Production of polyols and polyurethane from biomass: a review", Environmental Chemistry Letters **21** (2023) 2199. https://doi.org/10.1007/s10311-023-01592-4.

[7] E. Hornyák-Mester, M. Varga, L. M. Sőrés-Tölli, D. Mentes, A. F. Hatvani-Nagy, P. W. Groh, B. Viskolcz, G. Muránszky & B. Fiser, "Comparative analysis of thermal degradation effects on traditional and low-emission flexible polyurethane foams", Express Polymer Letters **18** (2024) 964. https://doi.org/10.3144/expresspolymlett.2024.74.

[8] M. C. Basso, S. Giovando, A. Pizzi, A. Celzard & V. Fierro, "Tannin/furanic foams without blowing agents and formaldehyde", Industrial Crops and Products **49** (2013) 17. https://doi.org/10.1016/j.indcrop.2013.04.043.

[9] N. Sultana, S. Z. Hossain, M. S. Alam, M. Hashish & M. Islam, "An experimental investigation and modeling approach of response surface methodology coupled with crow search algorithm for optimizing the properties of jute fiber reinforced concrete", Construction and Building Materials **243** (2020) 118216. https://doi.org/10.1016/j.conbuildmat.2020.118216.

[10] R. Feng, O. Y. C. Hou, H. Dai, Z. Cheng, Z. Deng & H. Gao, "Effect of glass fiber on the mechanical and thermal insulation performances of kaolinite-based thermal insulator", Case Studies in Construction Materials **21** (2024) e03879. https://doi.org/10.1016/j.cscm.2024.e03879.

[11] X. Wang, Y. Jin, Q. Ma & X. Li, "Performance and mechanism analysis of natural fiber-reinforced foamed concrete", Case Studies in Construction Materials **21** (2024) e03476. https://doi.org/10.1016/j.cscm.2024.e03476.

[12] A. F. Hatvani-Nagy, F. Kristály, B. Viskolcz & B. Fiser, "Polyurethane composite behavior influenced by the characteristics of the employed bentonite filler", Scientific Reports **15** (2025) 33418. https://doi.org/10.1038/s41598-025-18822-0.

[13] J. Li, M. Zor, X. Zhou, G. Du, D. Rodrigue & X. A. Wang, "Environmentally friendly tannic acid-furfuryl alcohol-soybean isolate/casein composite foams reinforced with wood fibers", Journal of Renewable Materials **13** (2025) 329. https://doi.org/10.32604/jrm.2024.056795.

[14] T. Varila, H. Romar, T. Luukkonen, T. Hilli & U. Lassi, "Characterization of lignin enforced tannin/furanic foams", Heliyon **6** (2020) e03228. https://doi.org/10.1016/j.heliyon.2020.e03228.

[15] A. J. Adebayo, J. K. Ogunjobi, O. O. Oluwasina & L. Lajide, "Development and characterization of lignin-furan rigid foams by varying precursors and catalyst concentration", International Journal of Environmental Science and Technology **21** (2024) 3087. https://doi.org/10.1007/s13762-023-05164-5.

[16] A. J. Adebayo, J. K. Ogunjobi, O. O. Oluwasina & L. Lajide, "Studies on the effect of additives concentrations on synthesis and characterization of furan-lignin foams", Current Research in Green and Sustainable Chemistry **6** (2023) 100362. https://doi.org/10.1016/j.crgsc.2023.100362.

[17] A. J. Adebayo & A. Olanrewaju, "A complete review of lignin's extraction, analysis, applications, and future outlook", Chemistry Africa **8** (2025) 1711. https://doi.org/10.1007/s42250-025-01323-y.

[18] G. C. D'Souza, H. Ng, P. Charpentier & C. C. Xu, "Recent developments in biobased foams and foam composites for construction applications", ChemBioEng Reviews **11** (2024) 7. https://doi.org/10.1002/cben.202300014.

[19] X. Zhou, B. Li, Y. Xu, H. Essawy, Z. Wu & G. Du, "Tannin-furanic resin foam reinforced with cellulose nanofibers (CNF)", Industrial Crops and Products **134** (2019) 107. https://doi.org/10.1016/j.indcrop.2019.03.052.

[20] Y. Chen, J. Yu, Y. Ling, S. Yao, X. Jiang, D. Hu, H. Wang & L. Zhao, "Comprehensive analysis of mechanical properties of microcellular polypropylene: experiment and simulation", Polymer Testing **116** (2022) 107812. https://doi.org/10.1016/j.polymertesting.2022.107812.

[21] B. Biswas, G. Grathoff, R. Naidu & L. N. Warr, "The multidisciplinary science of applied clay research: a 2021–2023 bibliographic analysis", Applied Clay Science **258** (2024) 107471. https://doi.org/10.1016/j.clay.2024.107471.

[22] A. J. Omotoyinbo, I. O. Oladele, J. M. Jabar, J. O. Borode, K. K. Alaneme, K. D. Akinwekomi, S. R. Oke, T. F. Omotosho & L. O. Saliu, "Comparative investigation of the influence of kaolin and dolomite on the properties of polyurethane foam", Manufacturing Review **8** (2021) 27. https://doi.org/10.1051/mfreview/2021025.

[23] A. M. Borrero-López, V. Nicolas, Z. Marie, A. Celzard & V. Fierro, "A review of rigid polymeric cellular foams and their greener tannin-based alternatives", Polymers **14** (2022) 3974. https://doi.org/10.3390/polym14193974.

[24] T. K. Fagbemigun & C. Mai, "Production and characterisation of self-blowing lignin-based foams", European Journal of Wood and Wood Products **81** (2023) 579. https://doi.org/10.1007/s00107-022-01908-1.

[25] M. B. Ferrer, A. Solt-Rindler, O. Vay, C. Hansmann & W. Gindl-Altmutter, "Bark based porous materials obtained with a simple mechanical foaming procedure", European Journal of Wood and Wood Products **81** (2023) 61. https://doi.org/10.1007/s00107-022-01856-w.

[26] X. Chen, X. Xi, A. Pizzi, E. Fredon, X. Zhou, J. Li, C. Gerardin & G. Du, "Preparation and characterization of condensed tannin non-isocyanate polyurethane (NIPU) rigid foams by ambient temperature blowing", Polymers **12** (2020) 750. https://doi.org/10.3390/polym12040750.

[27] X. Xi, A. Pizzi, C. Gerardin, H. Lei, X. Chen & S. Amirou, "Preparation and evaluation of glucose based non-isocyanate polyurethane self-blowing rigid foams", Polymers **11** (2019) 1802. https://doi.org/10.3390/polym11111802.

[28] J. Li, A. Zhang, S. Zhang, Q. Gao, W. Zhang & J. Li, "Larch tannin-based rigid phenolic foam with high compressive strength, low friability, and low thermal conductivity reinforced by cork powder", Composites Part B: Engineering **156** (2019) 368. https://doi.org/10.1016/j.compositesb.2018.09.005.

[29] A. Pizzi, "Tannin-based biofoams: a review", Journal of Renewable Materials **7** (2019) 477. https://doi.org/10.32604/jrm.2019.06511.

[30] K. Miedzińska, S. Członka, A. Strąkowska & K. Strzelec, "Biobased polyurethane composite foams reinforced with plum stones and silanized plum stones", International Journal of Molecular Sciences **22** (2021) 4757. https://doi.org/10.3390/ijms22094757.

[31] J. H. Grabber, C. Davidson, Y. Tobimatsu, H. Kim, F. Lu, Y. Zhu, M. Opietnik, N. Santoro, C. E. Foster, F. Yue, D. Ress, X. Pan & J. Ralph, "Structural features of alternative lignin monomers associated with improved digestibility of artificially lignified maize cell walls", Plant Science **287** (2019) 110070. https://doi.org/10.1016/j.plantsci.2019.02.004.

[32] M. C. Iacob, D. Popescu & F. Baciu, "Effect of process parameters on the hardness of 3D-printed thermoplastic polyurethane that includes foaming agent", Materials Plastics **60** (2024) 144. https://doi.org/10.37358/MP.23.4.5694.

[33] J. Li, S. Li, M. Zor, D. Rodrigue & X. A. Wang, "Biobased foam composites of tannic acid-furfuryl alcohol-furfural or vanillin reinforced with wood fibers", Industrial Crops and Products **226** (2025) 120726. https://doi.org/10.1016/j.indcrop.2025.120726.